Adsorption of fluids in disordered porous media from integral equation theory

C. Vega,[a] R. D. Kaminsky, and P. A. Monson[b]
Department of Chemical Engineering, University of Massachusetts, Amherst, Massachusetts 01003

(Received 22 February 1993; accepted 20 April 1993)

We consider the application of the integral equation theory developed by Madden and Glandt to a recently developed model of methane adsorbed in a silica xerogel. At higher temperatures, above the bulk fluid critical temperature, the theory yields very good predictions of the adsorbate–matrix and adsorbate–adsorbate distribution functions. At lower temperatures, where the attractive intermolecular forces play a more dominant role in determining the microstructure, the agreement between simulation and theory deteriorates somewhat. It also becomes increasingly difficult to obtain solutions of the integral equations at low temperatures. We have found that for this system and others where the matrix particles are much larger than the adsorbate particles the adsorbate–matrix and adsorbate–adsorbate correlation functions differ only slightly from those of an equilibrium mixture of matrix and adsorbate particles. We offer an explanation for this result on the basis of cancellation of diagrams in the cluster expansion of the total correlation function. We discuss the determination of adsorption isotherms from integral equation theory using expressions developed in the context of density functional theory.

I. INTRODUCTION

An important new approach to the understanding of fluid behavior in porous materials has recently been developed by Madden and Glandt[1,2] who considered the problem of determining distribution functions for fluids confined in random media such as heterogeneous porous materials. They treat the medium as a rigid array or matrix of obstacles with which the fluid molecules interact via some specified potential energy function. The approach leads to a theory of fluid structure in random media which is comparable in complexity to that of bulk fluid mixtures. Among the formal results they have obtained are a set of Ornstein–Zernike (OZ) equations for the distribution functions in the system. We will refer to these as the MGOZ equations. The MGOZ equations differ from those for an equilibrium mixture of fluid molecules and obstacles because the correlations between the obstacles are not influenced by interactions with the fluid molecules. The equations have been recently applied to hard sphere systems by Fanti *et al.*,[3] who have also presented density functional calculations[4] and Monte Carlo simulation results.[5]

The principal topic of the present paper is the application of MGOZ equations in the Percus–Yevick approximation to a molecular model representative of methane adsorbed in a silica xerogel, which was developed recently by Kaminsky and Monson.[6] The silica gel is modeled as a collection of spheres each composed of uniformly distributed Lennard-Jones interaction sites. The interaction between a Lennard-Jones adsorbate particle and one of these composite spheres leads to an analytic potential function, which is quite suited for use in the integral equation theory. The matrix of composite spheres is arranged to correspond to an equilibrium hard sphere configuration, which has been shown previously[7] to be a reasonable first approximation to the structure of silica gel. This system differs in two respects from the others to which the approach has been applied thus far. The first is that attractive adsorbate–matrix and adsorbate–adsorbate interactions are included so that the ability to treat these interactions is being tested for the first time. The second is that the matrix particles are very much larger than the adsorbate particles. This latter feature turns out to be of some importance since we are able to show that for large size differences between the matrix and adsorbate particles the microstructure of the adsorbate (as measured by the matrix–adsorbate and adsorbate–adsorbate distribution functions) is similar to that in an equilibrium mixture of matrix and adsorbate particles, provided that the structure of the matrix arises from matrix–matrix interactions which are short ranged and repulsive.

Recently Given and Stell[8] have pointed out that the MGOZ equations do not correspond to an entirely correct topological reduction of the cluster expansions of the total correlation function, except when particular closures such as the Percus–Yevick[9] (PY) or the mean spherical approximation[10] (MSA) are used to solve them. In order to construct the correct topological reduction it is necessary to decompose the fluid–fluid total and direct correlation functions into two contributions and when this is done a slightly different set of Ornstein–Zernike equations is obtained. If the MSA or PY closure is used then one of the contributions in this decomposition vanishes and the integral equations become functionally identical to the MGOZ equations.

[a]On leave from Departamento de Quimica-Fisica, Fac. CC. Quimicas, Université Complutense, 28040 Madrid, Spain.
[b]Author to whom correspondence should be addressed.

 0021-9606/93/99(4)/3003/11/$6.00

II. THEORY

The MGOZ equations relate the fluid–fluid, fluid–matrix, and matrix–matrix total correlation functions, $h_{ij}(r)=g_{ij}(r)-1$, and the direct correlation functions, $c_{ij}(r)$, via,

$$h_{mm}(r_{12})=c_{mm}(r_{12})+\rho_m\int c_{mm}(r_{13})h_{mm}(r_{32})d\mathbf{r}_3, \tag{1}$$

$$h_{mf}(r_{12})=c_{mf}(r_{12})+\rho_m\int c_{mm}(r_{13})h_{mf}(r_{32})d\mathbf{r}_3 +\rho_f\int c_{mf}(r_{13})C_{ff}(r_{32})d\mathbf{r}_3, \tag{2}$$

$$h_{fm}(r_{12})=c_{fm}(r_{12})+\rho_m\int c_{fm}(r_{13})h_{mm}(r_{32})d\mathbf{r}_3 +\rho_f\int c_{ff}(r_{13})h_{fm}(r_{32})d\mathbf{r}_3, \tag{3}$$

$$h_{ff}(r_{12})=c_{ff}(r_{12})+\rho_m\int c_{fm}(r_{13})h_{mf}(r_{32})d\mathbf{r}_3 +\rho_f\int c_{ff}(r_{13})h_{ff}(r_{32})d\mathbf{r}_3, \tag{4}$$

with $C_{ff}(r_{12})$ given by

$$C_{ff}(r_{12})=c_{ff}(r_{12})+\rho_f\int c_{ff}(r_{13})C_{ff}(r_{32})d\mathbf{r}_3, \tag{5}$$

where the subscripts m and f refer to the matrix and fluid respectively, and ρ_m and ρ_f are the number densities of matrix and fluid particles, respectively. These equations differ from those for an equilibrium mixture in two fundamental respects. In the MGOZ equations the matrix structure is not affected by the presence of the fluid whereas in the OZ equations it does. The second difference is the presence of $C_{ff}(r)$ in Eq. (2) instead of $h_{ff}(r)$ which appears in the OZ equations. This structure is required to prevent the appearance of shielding sets of matrix particle vertices in the graphs appearing in the cluster expansions of $h_{ff}(r)$ and $h_{fm}(r)$.[1]

In this work we use the Percus–Yevick[7] closure to solve the integral equations which can be written

$$c_{ij}(r)=[h_{ij}(r)+1]\{1-\exp[u_{ij}(r)/kT]\}, \tag{6}$$

where $u_{ij}(r)$ is the interaction potential between species i and j, with i or j denoting m or f as appropriate.

III. THERMODYNAMIC PROPERTIES FROM INTEGRAL EQUATION THEORY

The configurational internal energy of the adsorbed fluid can be readily computed from the knowledge of $g_{fm}(r)$ and $g_{ff}(r)$ as[1]

$$U_f/N_f=U_{ff}/N_f+U_{fm}/N_f =\frac{\rho_f}{2}\int u_{ff}(r)4\pi r^2 g_{ff}(r)dr +\rho_m\int u_{fm}(r)4\pi r^2 g_{fm}(r)dr. \tag{7}$$

The Henry's constant, K_H, is given by

$$K_H=\lim_{z_f\to 0}\frac{\rho_f}{z_f}=\exp(-\mu_f^{\mathrm{res},\infty}/kT) \tag{8}$$

where z_f is the activity of the fluid, so that the problem here is to compute the residual chemical potential of the fluid in the porous material at infinite dilution, $\mu_f^{\mathrm{res},\infty}$. In this work $u_{mm}(r)$ is always a hard sphere potential. If $u_{fm}(r)$ contains both attractive and repulsive forces we can obtain K_H using a perturbation scheme based on the coupling parameter method of Kirkwood[11] and using a hard sphere mixture as the reference state. If we define $u_{fm}(r,\lambda)=\lambda u_{fm}(r)$ then,

$$-\ln(K_H)=\frac{\mu_f^{\mathrm{res},\infty}}{kT} \approx\frac{\mu_H^{\mathrm{res},\infty}}{kT}+\frac{\rho_m}{kT}\int_{\lambda_{\min}}^1 d\lambda\int_0^\infty u_{fm}(r) \times g_{fm}(r,\rho_m,\rho_f=0,T,\lambda)4\pi r^2\,dr, \tag{9}$$

where $\lambda_{\min}$ is a small value of λ and $\mu_H^{\mathrm{res},\infty}$ is the residual chemical potential at infinite dilution of a hard particle fluid in a "solvent" of hard matrix particles. This method resembles the use of perturbation theory to obtain K_H in bulk binary mixtures. The integrand of Eq. (9) is obtained by solving the MGOZ equations with $\rho_f=0$.

The determination of other thermodynamic properties in these systems is not quite so straightforward. Of particular importance is the adsorption isotherm which describes how the average density of the adsorbed fluid changes with changes in properties (pressure or chemical potential) of the bulk fluid at constant temperature. Since we are using a theory in which the average density of the fluid in the porous material is fixed we must determine a relationship between the chemical potential and this average density to obtain the absorption isotherm. Fanti *et al.*[3–5] have suggested that an appropriate route to this is to calculate the pressure of the fluid in the porous material via a virial theorem and then to obtain the chemical potential via integration of the isothermal Gibbs–Duhem equation. Their expression for the virial pressure is[3–5]

$$P_m=\rho_f kT-\frac{\rho_f^2}{6}\int d\mathbf{r}\, r\frac{du_{ff}(r)}{dr}g_{ff}(r) -\frac{\rho_f\rho_m}{3}\int d\mathbf{r}\, r\frac{du_{fm}(r)}{dr}g_{fm}(r). \tag{10}$$

This equation has the same form as the virial pressure for an equilibrium mixture but without the matrix–matrix contribution. Unfortunately, as we will show later, using

Monte Carlo simulation results for a specific example, this virial route yields results for the adsorption isotherm which are inconsistent with those determined directly in the Monte Carlo simulation. We return to this issue in more detail later. As an alternative to the virial route we have developed two other theoretical routes to the adsorption isotherm which are based upon the equations of density functional theory.

The Madden–Glandt formalism[1] starts by treating a macroscopic sample of the adsorbent as being divided into a very large number of subsamples, each of volume V, with different numbers of matrix particles in different spatial configurations. The distribution of numbers of matrix particles and their configurations follow a probability determined by the hierarchy of distribution functions of the matrix particles. The thermodynamics of adsorption in the supramacroscopic sample of the porous material can be described by starting from a fundamental equation of state in the grand potential representation, as can adsorption in any of the realizations of the matrix. The grand potential of the fluid adsorbed in the supramacroscopic system is the sum of the grand potentials for the subsamples, and the grand potential per unit volume is the average of the grand potential per unit volume over the distribution of subvolumes. The grand potential per unit volume of adsorbent, Ω_f, is related to the adsorbate density and the chemical potential (at constant volume and temperature) via the Gibbs–Duhem equation

$$d\Omega_f=\rho_f\, d\mu_f. \tag{11}$$

It should be noted that the quantity P_m in the Gibbs–Duhem equation of Fanti *et al.*[3–5] and in Eq. (10) is equivalent to Ω_f. In our approach we first use the equations of density functional theory to express the grand potential for an individual realization of the matrix and then perform the average over the realizations to obtain expressions cast in terms of the correlation functions obtainable from the MGOZ equation.

Let us focus on a single configuration of the matrix particles denoted by $\mathbf{q}^M$. The inhomogeneous density of the fluid for this particular realization is given by $\hat{\rho}_f(\mathbf{r}_1;\mathbf{q}^M)$ where $\mathbf{r}_1$ denotes the position of a fluid molecule. Let us imagine a charging process of the fluid into the porous medium from zero density to the final density distribution so that $\hat{\rho}_f(\mathbf{r}_1,\lambda;\mathbf{q}^M)=\lambda\hat{\rho}_f(\mathbf{r}_1;\mathbf{q}^M)$ or simply $\lambda\hat{\rho}_f$ with λ varying from zero to one. We may write the grand potential for a specific realization of the matrix as[13,14]

$$\Omega_f(\mathbf{q}^M)=\frac{kT}{V}\int\hat{\rho}_f(\mathbf{r}_1;\mathbf{q}^M)d\mathbf{r}_1\Big[\int_0^1\lambda d\lambda \times\int d\mathbf{r}_2\,\hat{\rho}_f(\mathbf{r}_2;\mathbf{q}^M)\hat{c}_{ff}(\mathbf{r}_1,\mathbf{r}_2;\lambda\hat{\rho}_f)-1\Big], \tag{12}$$

where $\hat{c}_{ff}(\mathbf{r}_1,\mathbf{r}_2;\lambda\hat{\rho}_f)$ is the direct correlation function for the inhomogeneous system when the singlet density is $\lambda\hat{\rho}_f$. Let us now define the operator $\bar{o}$,

$$\bar{o}A=\sum_{M=0}^{\infty}\frac{P_M}{M!}\int AP^M(\mathbf{q}^M)d\mathbf{q}^M \tag{13}$$

with the property that $\bar{o}\,1=1$. Here P_M is the probability distribution for numbers of matrix particles in the subvolumes and $P^M(\mathbf{q}^M)d\mathbf{q}^M$ is the probability of observing a given configuration of M matrix particles. Evidently, $\bar{o}$ performs the operation of averaging any property over all realizations of the matrix with the appropriate probability. Applying the operator $\bar{o}$ to both sides of Eq. (12) and using the approximation

$$\bar{o}\hat{c}_{ff}(\mathbf{r}_1,\mathbf{r}_2;\lambda\hat{\rho}_f)=c_{ff}(r_{12};\lambda\rho_f), \tag{14}$$

we obtain

$$\Omega_f\approx\rho_f kT\Big[-1+\frac{1}{\rho_f}\int_0^{\rho_f}\tilde{c}_{ff}(k=0,\rho_f')\rho_f'\,d\rho_f'\Big], \tag{15}$$

where $\tilde{c}_{ff}(k)$ is the Fourier transform of $c_{ff}(r)$. Equation (15) is quite simple and reduces to the compressibility equation of state for the bulk fluid. It may prove possible to evaluate the integral over density in Eq. (15) analytically in the Percus–Yevick approximation by extending the method developed by Baxter[12] for bulk mixtures, although we have not done this.

The chemical potential $\mu_f(\mathbf{q}^M)$ for a single realization of the matrix can be written as[13,14]

$$\begin{aligned}N_f\mu_f(\mathbf{q}^M)=&kT\int\hat{\rho}_f(\mathbf{r}_1;\mathbf{q}^M)\ln[\Lambda_f^3\hat{\rho}_f(\mathbf{r}_1;\mathbf{q}^M)]d\mathbf{r}_1\\&+\int V_{\text{ext}}(\mathbf{r}_1;\mathbf{q}^M)\hat{\rho}_f(\mathbf{r}_1;\mathbf{q}^M)d\mathbf{r}_1\\&-kT\int_0^1 d\lambda\int d\mathbf{r}_1\int d\mathbf{r}_2\,\hat{\rho}_f(\mathbf{r}_1;\mathbf{q}^M)\\&\times\hat{\rho}_f(\mathbf{r}_2;\mathbf{q}^M)\hat{c}_{ff}(\mathbf{r}_1,\mathbf{r}_2;\lambda\hat{\rho}_f),\end{aligned} \tag{16}$$

where Λ_f is the de Broglie wavelength and V_{ext} is the external field. In our case the external field for the fluid particles is just the field created by the presence of the matrix particles. The chemical potential does not depend on $\mathbf{q}^M$ since for any realization of the matrix the bulk fluid with chemical potential μ_f is in equilibrium with the fluid adsorbed in the matrix. Now applying the operator to both sides of Eq. (16) we have

$$N_f\mu_f=\bar{o}R_1+\bar{o}R_2+\bar{o}R_3, \tag{17}$$

where R_1, R_2, and R_3 refer to the terms on the right-hand side of Eq. (16). It is interesting to point out that when the averaged fluid density ρ_f goes to zero and the rigorous value of $\hat{\rho}_f$ in this limit is substituted in Eq. (17) then Eq. (8) is obtained. Let us now analyze each of the three terms of Eq. (17). The second term of the right-hand side ($\bar{o}R_2$) reduces to the contribution to the internal energy from the fluid–matrix interaction

$$\bar{o}R_2=N_f\rho_m\int u_{fm}(r)g_{fm}(r)4\pi r^2\,dr=U_{fm}. \tag{18}$$

Let us now focus on the $\bar{o}R_3$ term. At the same level of approximation used in developing Eq. (15) we have

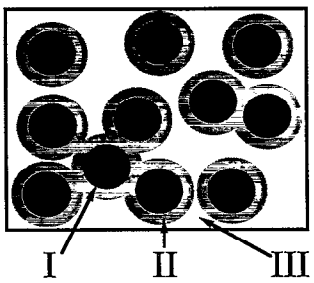

FIG. 1. The three regions of the integrand in Eq. (20). The radius of the sphere involving region I and II around each matrix particle is L_2.

$$\bar{o}R_3 \approx -kT \int_0^1 d\lambda \int d\mathbf{r}_1 \int d\mathbf{r}_2\, c_{ff}(r_{12},\lambda\rho_f)\rho_f\rho_f$$

$$= -N_f kT \int_0^{\rho_f} \tilde{c}_{ff}(k=0,\rho_f')d\rho_f'. \tag{19}$$

For an homogeneous fluid Eq. (19) is just the compressibility route to the residual chemical potential.

Let us now focus on the $\bar{o}R_1$ term. This term can be alternatively regarded as the spatial average of $\hat{\rho}_f \ln(\hat{\rho}_f)$ over all realizations of the fluid. It reduces to the chemical potential of an ideal gas in the limit of a homogeneous system. We propose to approximate it with its value for a single realization, i.e.,

$$\bar{o}R_1 = kT \int \hat{\rho}_f(\mathbf{r}) \ln[\hat{\rho}_f(\mathbf{r})]d\mathbf{r} = N_f \mu_f^{\text{ideal}}. \tag{20}$$

Our justification for this is that for a sufficiently large subvolume we can expect this quantity to vary little between different realizations of the matrix. The integrand in Eq. (20) is familiar in density functional theory treatments. It appears in applications of density functional theory to adsorption in idealized geometries,[15] in the treatment of freezing,[16] and in the treatment of liquid crystal phases.[17] In all these treatments the function $\hat{\rho}_f$ is readily obtained so that the integral of Eq. (20) can be computed. However, the present situation is not quite so simple due to the lack of symmetry of the integrand. In this work we have explored a simple intuitive idea which should provide a reasonable estimate of this term. The terminology μ_f^{ideal} has been used in Eq. (20) since for a homogeneous system it reduces to $kT \ln \rho_f$.

If the fluid density was uniform then the $\bar{o}R_1$ term would have its minimum value (namely, $N_f kT \ln \rho_f$) and any inhomogeneity will increase the value. We have therefore a rigorous lower bound for μ_f^{ideal} since $\mu_f^{\text{ideal}} \geqslant kT \ln \rho_f$. Moreover an analysis of the density distribution reveals the presence of three different regions (see Fig. 1). Region I represents the space excluded to the fluid particles due to the presence of the matrix particles. Region II represents an adsorbed monolayer of fluid particles situated on the surface of the matrix particles and corresponds to the first peak in $g_{fm}(r)$. In region III we shall assume that the inhomogeneity is small (a severe approximation) and that the contribution from this region is given by $\rho^{\text{III}} \ln \rho^{\text{III}}$. The value of $\bar{o}R_1$ estimated by integrating through these three regions and neglecting any possible overlap between regions I and II is obtained from

$$\bar{o}R_1 = N_f kT \left\{ \rho_m \int_0^{L_2} g_{fm}(r) \ln[\rho_f g_{fm}(r)] 4\pi r^2\, dr + \ln(\rho^{\text{III}}) \left[1 - \rho_m \int_0^{L_2} g_{fm}(r) 4\pi r^2\, dr \right] \right\}, \tag{21}$$

where

$$\rho^{\text{III}} = \frac{\rho_f}{(1-\rho_{m\frac{4}{3}}\pi L_2^3)} \left[1 - \rho_m \int_0^{L_2} g_{fm}(r) 4\pi r^2\, dr \right]. \tag{22}$$

The choice of L_2 which separates regions II and III is somewhat arbitrary although it is subject to two constraints. It should represent the average fluid–matrix distance of a fluid molecule adsorbed on the surface of the matrix particles and it should guarantee a positive value for ρ^{III}. In this work we shall choose L_2 close to the first minimum of the $g_{fm}(r)$. The final expression of the chemical potential is

$$\mu_f/kT = \mu_f^{\text{ideal}}/kT + \rho_m \int u_{fm}(r) g_{fm}(r) 4\pi r^2\, dr - \int_0^{\rho_f} \tilde{c}_{ff}(k=0,\rho_f')d\rho_f'$$

$$= \mu^{(1)}/kT + \mu^{(2)}/kT + \mu^{(3)}/kT \tag{23}$$

with μ_f^{ideal} given by Eqs. (20)–(22). We will present results for adsorption isotherms based on the two routes, Eq. (15) and Eq. (23). We anticipate that they may not yield consistent results due both to the use of the Percus–Yevick approximation for $g_{fm}(r)$ and $c_{ff}(r)$, and to the assumptions used in deriving the two expressions from the equations of density functional theory.

IV. MODEL POTENTIALS AND NUMERICAL METHODS

The first model system we have considered, which has been previously described in detail in Ref. 6 is a model of methane adsorbed in a microporous silica gel, is given by

$$u_{ff}(r) = 4\epsilon \left[\left(\frac{\sigma}{r}\right)^{12} - \left(\frac{\sigma}{r}\right)^{6} \right], \tag{24}$$

$$u_{mm}(r) = u_{HS}(r;D) \quad D = 2R = 7.055\sigma, \tag{25}$$

$$u_{fm}(r) = \infty \quad r \leqslant R, \tag{26}$$

$$= \frac{16}{3}\pi\rho_s R^3 \epsilon_{gs} \left[\frac{(r^6 + 21/5 r^4R^2 + 3r^2R^4 + R^6/3)\sigma_{gs}^{12}}{(r^2-R^2)^9} - \frac{\sigma_{gs}^6}{(r^2-R^2)^3} \right] \quad r > R, \tag{27}$$

where $\epsilon/k = 148.2$ K, $\sigma = 0.3817$ nm, $R = 1.346$ nm, $\sigma_{gs} = 0.33$ nm, $\rho_s = 44$ nm^{-3}, and $\epsilon_{gs}/k = 339$ K. For convenience we call this model M1. The fluid–matrix potential is the composite sphere potential of Kaminsky and Monson[6]

with parameters chosen to model the methane–silica interaction. The packing fraction of the matrix particles $\eta_m = \pi/6\ \rho_m D^3$ is 0.386 for all the systems studied. The value of $u_{fm}(r)$ at the minimum is about -6ϵ. The second model we consider consists of a fluid of hard spheres of diameter σ and a matrix of hard spheres of diameter $D=7.055\sigma$ with a packing fraction $\eta_m=0.386$ and with additive diameters for the cross interaction. We will refer to this model as M2. The third model considered is a fluid of hard spheres of diameter σ in a matrix of hard spheres of diameter $D=3\sigma$ with $\eta_m=0.25$. We will refer to this model as M3.

We have solved the MGOZ with the PY closure for the the three models described above using a slight modification of the algorithm of Labik *et al.*[18–20] for solving the OZ for an equilibrium binary mixture. In our numerical work we used 4096 data points for each of the correlation functions with a grid size of $\Delta r=0.004\sigma$. This rather fine grid was necessitated by the quickly varying behavior of $g_{fm}(r)$ for the M1 model in the neighborhood of the $u_{fm}(r)$ collision diameter. For each density of the fluid we started by solving the MGOZ at high temperatures and then proceeded to lower temperatures taking the previous solution as the initial guess. Proceeding in this way the convergence was found to be fast.

Throughout this paper we will use the following reduced units defined by:

$$\rho_f^*=\rho_f\sigma^3;\ z_f^*=\rho_f^*\exp(\mu_f^{\rm res}/kT);\ T^*=kT/\epsilon. \quad (28)$$

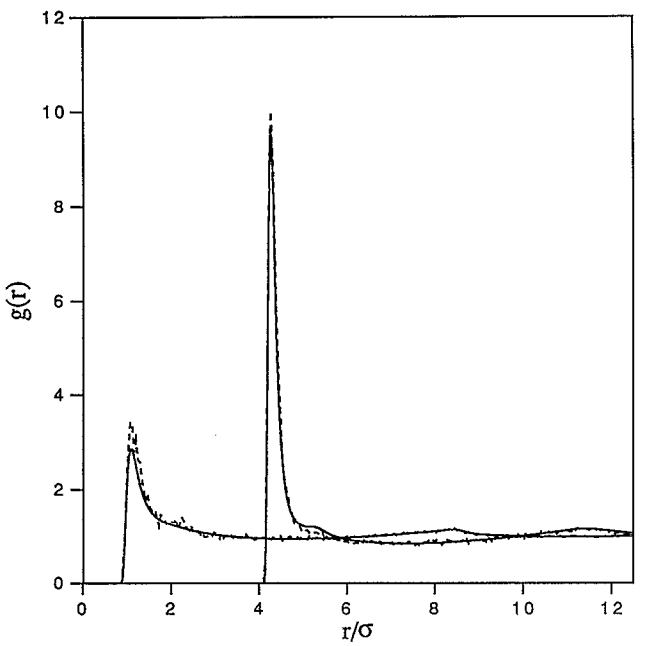

FIG. 2. Fluid–fluid distribution function $g_{ff}(r)$ and fluid–matrix distribution function $g_{fm}(r)$ for the M1 model with $T^*=2$ as obtained from MGOZ integral equation (solid line) and from GCMC simulations (dashed line). The distribution functions from left to the right are $g_{ff}(r)$ and $g_{fm}(r)$, respectively, and $\rho_f^*=0.0299$.

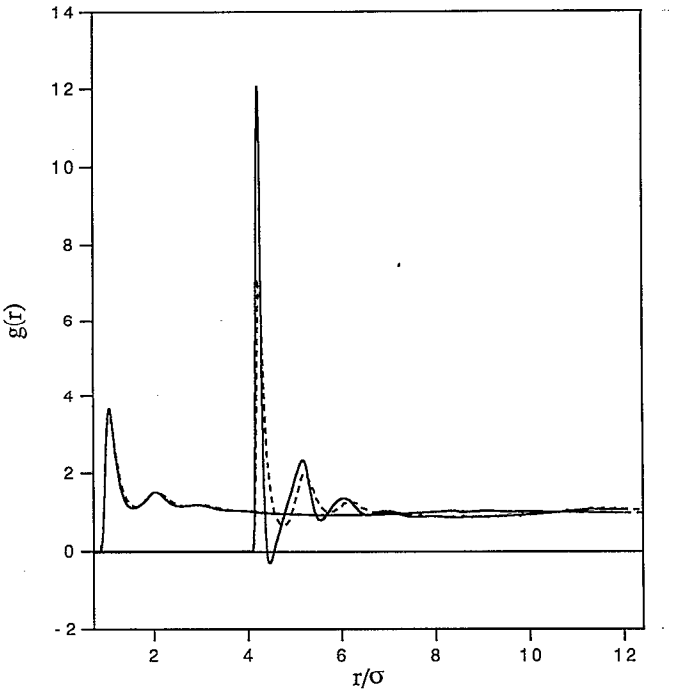

FIG. 3. Fluid–fluid distribution function $g_{ff}(r)$ and fluid–matrix distribution function $g_{fm}(r)$ for the M1 model with $T^*=2$ as obtained from MGOZ integral equation (solid line) and from GCMC simulations (dashed line). The distribution functions from left to the right are $g_{ff}(r)$ and $g_{fm}(r)$, respectively, and $\rho_f^*=0.3593$.

V. DISTRIBUTION FUNCTIONS, INTERNAL ENERGIES, AND HENRY'S CONSTANTS

We begin this section by considering the results obtained for the M1 model. For this model there are previously reported grand canonical Monte Carlo (GCMC) results.[6] In these simulations and in the solutions of the MGOZ equations $u_{ff}(r)$ was truncated at $r=2.5\sigma$. Figures 2 and 3 shows the results for $T^*=2$ at two values of the average density. The agreement for the low density is remarkably good, especially taking into account the high values of the first peaks of the pair distribution functions. The position of the peaks is correctly predicted and also the presence of a cusp in the $g_{ff}(r)$ function. The physics underlying these features of the distribution functions are discussed in detail in Refs. 6 and 21. At the highest density, although the results for $g_{ff}(r)$ are quite good, the description of $g_{fm}(r)$ fails. The height of the first peak is overemphasized and the first minimum takes nonphysical negative values. Negative values of the first minimum are also found in the wall-fluid OZ equation at high densities.[22] We interpret this result as a failure of the PY closure when the size ratio between the particles is large and the attractive interactions between the matrix and adsorbate particles very strong. In Figs. 4 and 5 we show the results for $T^*=1.2$ at two densities. The quality of the theoretical predictions is somewhat poorer than those at $T^*=2$. However, the positions and heights of the peaks is still predicted reasonably well. For the highest activity the description of the first peak and first minimum is poor again giving negative val-

ues for $g_{fm}(r)$. Comparisons at $T^*=1.0$ lead to similar conclusions. However, at the higher densities at this temperature $h_{ff}(r)$ becomes very long ranged and beyond a certain density we were not able to obtain solutions. In Fig. 6 we show the results for $T^*=1$ for $g_{ff}(r)$ at the highest density where a solution was possible and simulation data was available. Notice that the $g_{ff}(r)$ from simulation decays in a very different way than the theoretical result. One possible interpretation of these results may be as an indication of criticality of the adsorbed fluid. Such long range correlations can be seen in solutions of the Percus–Yevick theory for the 12-6 potential in the bulk near the critical point.[23] However, it should be pointed out that no indication of any phase transition was observed in the GCMC simulations[6] of the M1 model for the temperatures studied ($T^*>0.80$). Finally, except at very low densities we were not able to obtain solutions to the MGOZ equations for $T^*<1$. All together the agreement for the M1 model is satisfactory although some deficiencies are evident. Of course from a practical perspective it should be emphasized that adsorption in silica gels is most often used at supercritical temperatures of the bulk fluid. In that respect the results for $T^*=2.0$ for the M1 model are especially encouraging.

We now consider the results for the internal energy. In Table I we show the results for $T^*=2$ and 1.2 as obtained from GCMC and from Eq. (7) together with the MGOZ equation for the distribution functions. The results are satisfactory. The theory in general yields less negative values of the internal energy than the simulation. The theoretical results for the fluid–fluid contribution to the internal energy are better than those of the fluid–matrix interaction which can be readily understood from our previous discussion of the structural results. U_f/N_f decreases as the density of the fluid in the porous media increases. This is analogous to the behavior of a bulk fluid. However, U_{fm}/N_f increases as the density of the fluid increases. This is

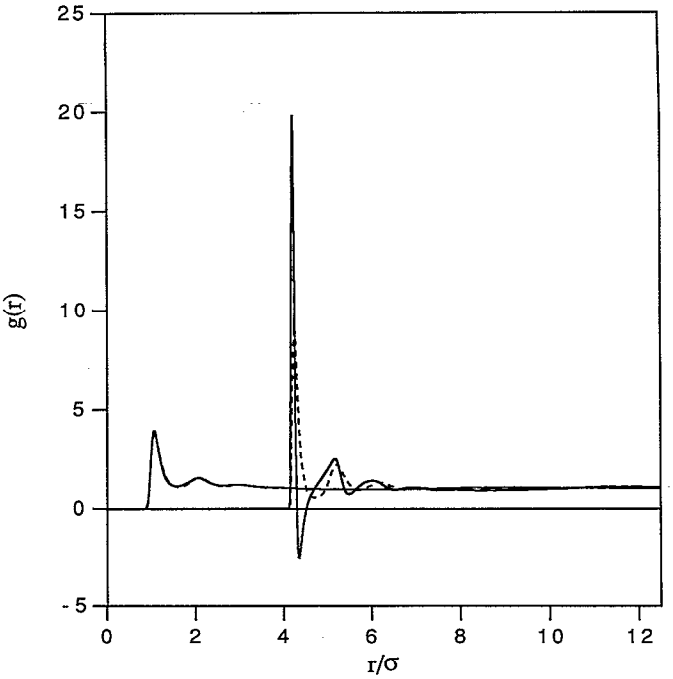

FIG. 5. Fluid–fluid distribution function $g_{ff}(r)$ and fluid–matrix distribution function $g_{fm}(r)$ for the M1 model with $T^*=1.2$ as obtained from MGOZ integral equation (solid line) and from GCMC simulations (dashed line). The distribution functions from left to the right are $g_{ff}(r)$ and $g_{fm}(r)$, respectively, and $\rho_f^*=0.3534$.

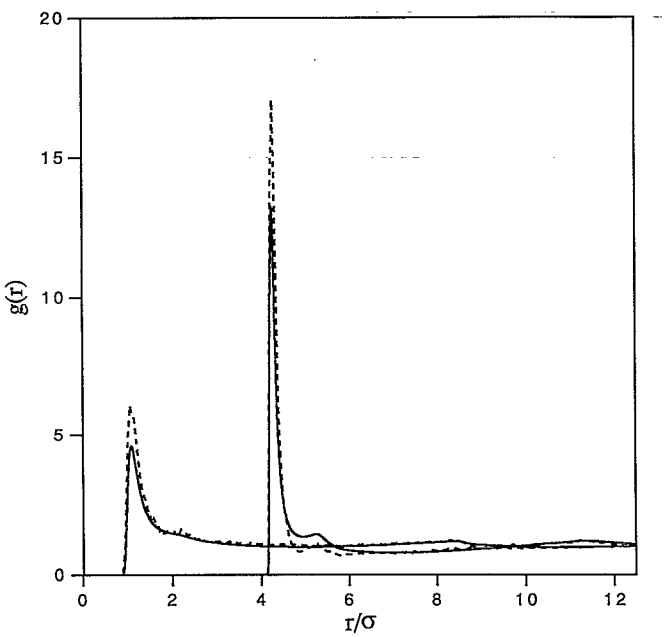

FIG. 4. Fluid–fluid distribution function $g_{ff}(r)$ and fluid–matrix distribution function $g_{fm}(r)$ for the M1 model with $T^*=1.2$ as obtained from MGOZ integral equation (solid line) and from GCMC simulations (dashed line). The distribution functions from left to the right are $g_{ff}(r)$ and $g_{fm}(r)$, respectively, and $\rho_f^*=0.0384$.

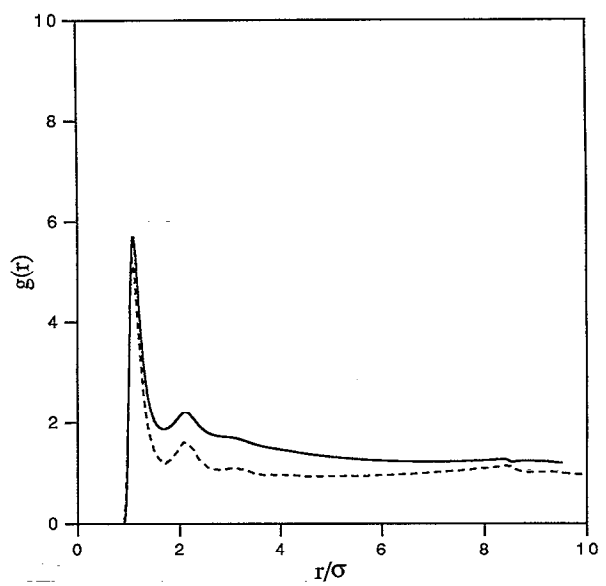

FIG. 6. Fluid–fluid distribution function $g_{ff}(r)$ for the M1 model with $T^*=1.0$ and $\rho_f^*=0.1526$ as obtained from MGOZ integral equation (solid line) and from GCMC simulations (dashed line).

TABLE I. Fluid–fluid, U_{ff}, and fluid–matrix, U_{fm}, contribution to the internal energy for the M1 model as obtained from MGOZ and Eq. (7) and from the GCMC simulations of Ref. 6.

T^*	z_f^*	ρ_f^*	U_{ff}/N_fkT GCMC	U_{ff}/N_fkT Theory	U_{fm}/N_fkT GCMC	U_{fm}/N_fkT Theory
2	7.738×10^{-3}	0.0299	−0.151	−0.138	−3.350	−3.174
2	7.738×10^{-2}	0.1696	−0.736	−0.728	−2.592	−2.470
2	1.393	0.3593	−1.545	−1.515	−2.156	−2.178
1.2	7.738×10^{-4}	0.0384	−0.516	−0.425	−7.267	−6.001
1.2	7.738×10^{-3}	0.1805	−1.619	−1.522	−5.267	−4.092
1.2	4.640×10^{-2}	0.3534	−2.817	−2.797	−3.928	−3.651

due to the fact that when the surface of the matrix saturates with fluid particles, the additional fluid molecules are adsorbed in a second layer where the fluid–matrix interactions are considerably weaker. Interestingly the total internal energy, $U_{ff}+U_{fm}$, depends only weakly on the total amount of fluid adsorbed.

The Henry's constant has also been determined from the MGOZ results plus the perturbation scheme of Eq. (9) with $\lambda_{\min}=0.005$. To relate the M1 model with $\lambda_{\min}$ to an equivalent hard body system we have assigned a hard-body diameter to the fluid–matrix interaction D_{fm} by using the Barker–Henderson prescription[24] applied to the potential $\lambda_{\min}\, u_{fm}(r)$. Since D is known, once D_{fm} is determined $\mu_H^{\rm res}$ can be easily computed from the equation of state of mixtures of hard spheres proposed by Mansoori *et al.*[25,26] One hundred values of λ were used in the numerical integration of Eq. (9). The values of the Henry's constant of the M1 model as estimated in this way are shown in Table II along with values computed from Monte Carlo integration.[6] The agreement is very good except for the lowest temperature ($T^*=0.80$). It should be stressed that the prediction of Henry's constant even in equilibrium binary mixtures with large size ratios is a difficult problem and has been discussed in several studies.[27,28] The results of Table II which involve a diameter ratio of ~ 7, as well as a very strong cross interaction can be therefore regarded as satisfactory.

We now present some results for the M2 model of hard spheres in a hard sphere matrix. The M2 model can be regarded as the hard sphere version of the M1 model. We have again solved the MGOZ equations for several values of the fluid density. Moreover since there are not previously reported simulation data for this system or for the M3 model we have performed several GCMC simulations. The details of the simulations are similar to those of Ref. 6.

TABLE II. Henry's constants K_H for the M1 model as estimated from the MGOZ equations via Eq. (9) and as computed from the Monte Carlo integration of Ref. 6.

T^*	MC $\ln(K_H)$	Theory $\ln(K_H)$
2	1.49	1.54
1.2	4.37	4.26
1	6.19	5.77
0.8	9.34	8.10

We took an equilibrium configuration from a 32 particle system of hard spheres ($\eta_m=0.386$) to mimic the porous medium created by the matrix particles in model M1. We then used GCMC for three different values of the activity of the fluid. The results for the average density vs activity are shown in Table III. In Fig. 7 we show $g_{ff}(r)$ and $g_{fm}(r)$ as obtained from the GCMC simulations and from the MGOZ equation for the M2 model. The agreement is remarkably good. The contact values from the integral equation are slightly lower than those from simulation. This behavior is typical of the PY closure when applied to equilibrium hard sphere systems. By comparing Fig. 7 with Fig. 2 or Fig. 3 we can obtain an idea of the effect of the attractive forces on the structure of the fluid in the porous medium. In general the position of the peaks and the general shape is the same, although the attractive forces (especially the strong fluid–matrix interaction) in model M1 enhances the height of the first peak substantially. Similar good agreement between simulation and theory was found for the M3 model also.

We have also investigated how the results of the MGOZ equations differ from those of an equilibrium binary mixture obtained by solving the OZ equations. First we explored hard spheres of diameter σ in a matrix of hard spheres of diameter D/σ. In Fig. 8 we show the results for

TABLE III. GCMC results for adsorption of a fluid of hard spheres of diameter σ in a matrix of hard spheres diameter D. The packing fraction of the fluid η_f is defined as $\eta_f=\pi/6\ \rho_f^*$.

D/σ	η_m	z_f^*	η_f
7.055	0.386	0.10	0.0171
7.055	0.386	1.00	0.0649
7.055	0.386	10.0	0.1218
3.000	0.250	0.01	0.0022
3.000	0.250	0.03	0.0063
3.000	0.250	0.10	0.0178
3.000	0.250	0.20	0.0297
3.000	0.250	0.30	0.0385
3.000	0.250	0.70	0.0607
3.000	0.250	1.00	0.0710
3.000	0.250	3.00	0.1038
3.000	0.250	10.0	0.1382
3.000	0.250	30.0	0.1662
3.000	0.250	100.0	0.1933
3.000	0.250	300.0	0.2149
3.000	0.250	1000.0	0.2349
3.000	0.250	3000.00	0.2512

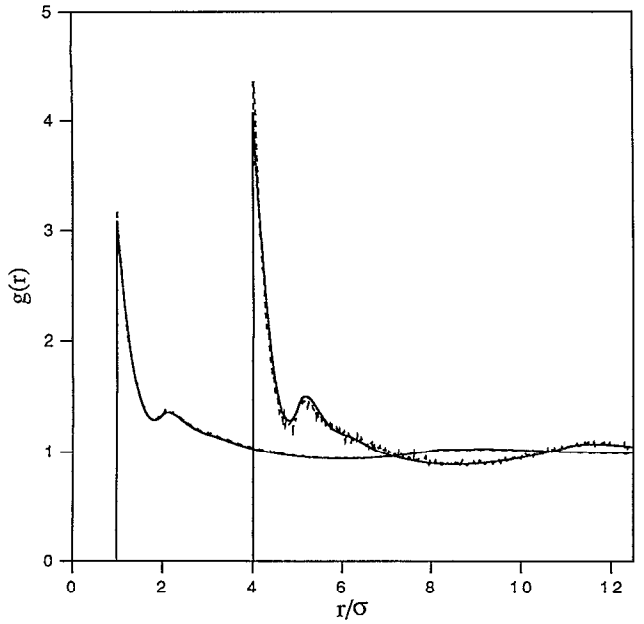

FIG. 7. Fluid–fluid distribution function $g_{ff}(r)$ and fluid–matrix distribution function $g_{fm}(r)$ for the M2 model (D/σ=7.055, η_m=0.386) as obtained from MGOZ integral equation (solid line) and from GCMC simulations (dashed line). The distribution functions from left to right are $g_{ff}(r)$ and $g_{fm}(r)$, respectively, and $\rho_f^* = 0.2336$.

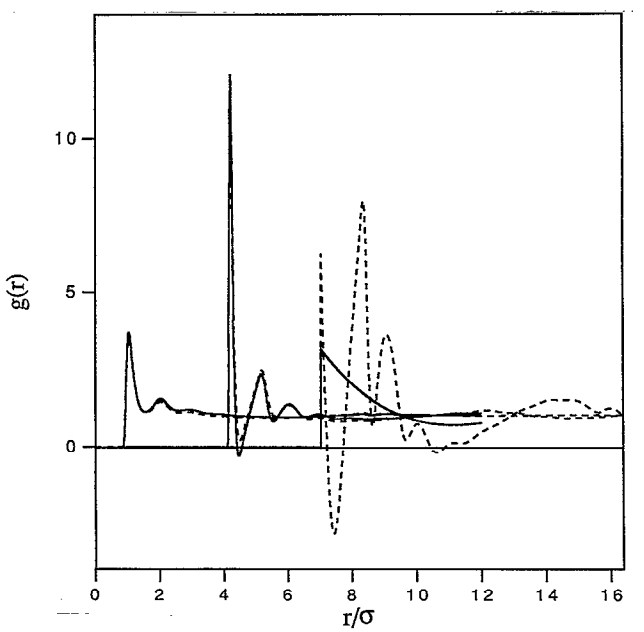

FIG. 9. Structure of the M1 model with T^*=2 as obtained from the MGOZ equations (solid line) and from the OZ equations for a binary mixture with the PY closure (dashed line). The distribution functions from left to right are $g_{ff}(r)$, $g_{fm}(r)$, and $g_{mm}(r)$, and $\rho_f^* = 0.3593$.

the M2 model. We see that the $g_{ff}(r)$ and $g_{fm}(r)$ for the fluid adsorbed in the porous material and for the equilibrium binary mixture are almost identical. Of course $g_{mm}(r)$ differs significantly in both system since in the equilibrium

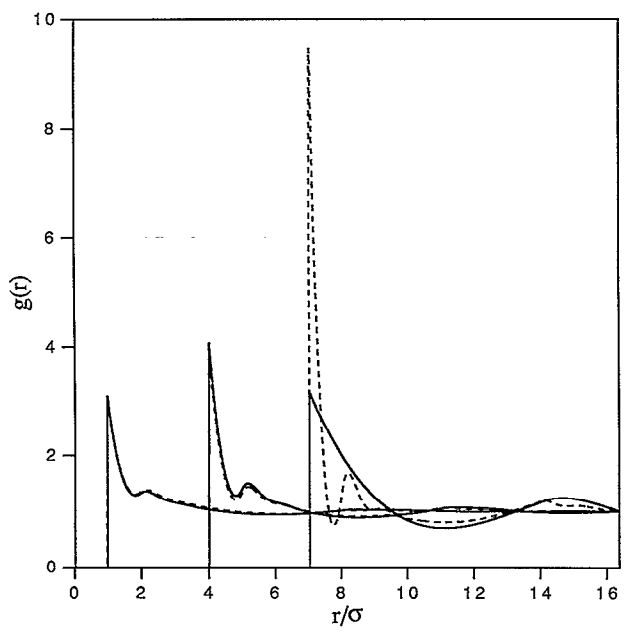

FIG. 8. Distribution functions for the M2 model (D/σ=7.055, η_m =0.386) with $\rho_f^* = 0.2336$ as obtained from the solution of the MGOZ equation (solid line) and from the OZ equation for a binary mixture with the PY closure (dashed line). The distribution functions from left to the right are the $g_{ff}(r)$, $g_{fm}(r)$, and $g_{mm}(r)$.

mixture the structure of the matrix is affected by the presence of the fluid whereas in the porous material the structure of the matrix is rigid and cannot be affected by the presence of the fluid. Our conclusion after analyzing many other results not shown here for different size ratios is that $g_{ff}(r)$ and $g_{fm}(r)$ for the porous medium and for the binary mixture are almost undistinguishable when the size ratio of the matrix particles to the fluid particles is substantially greater than unity. For smaller size ratios $g_{ff}(r)$ and $g_{fm}(r)$ in the porous medium and in the equilibrium binary mixture differ considerably.[4] Note that in the porous medium the roles of fluid and matrix particles are not symmetric (unlike the case of a binary mixture) and therefore the behavior of the system with $D^*=3$ differs enormously of the system $D^*=1/3$ when the volume fractions of fluid and matrix particles are kept constant. The similarity between quenched medium and equilibrium binary mixture is not restricted to hard particles. In Fig. 9 we show $g_{ff}(r)$, $g_{fm}(r)$, and $g_{mm}(r)$ for the system M1 with T^*=2 at one fluid density. Again $g_{ff}(r)$ and $g_{fm}(r)$ are almost indistinguishable between the two systems. Of course the behavior of $g_{mm}(r)$ is very different in both cases. Interestingly the peaks of $g_{mm}(r)$ in the binary mixture are separated by a distance of σ, and moreover the oscillations are typical of the solvent induced force between two planar walls immersed in a fluid.[29]

To a significant extent we can explain the similarity between the fluid–fluid and fluid–matrix distribution functions of the equilibrium mixture and the quenched–annealed (adsorption) system in terms of the diagramatic expansions. The difference between the expansions for the quenched–annealed system and for the equilibrium mix-

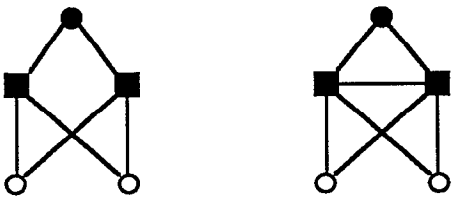

FIG. 10. Cluster diagrams with shielding sets of matrix vertices (squares) appearing the cluster expansion of the total correlation function $h_{ff}(r)$ for an equilibrium mixture of adsorbate particles and matrix particles. The conventions used for definition of bonds and vertices is that described by Madden and Glandt (Ref. 1). For hard sphere interactions between the matrix particles these two diagrams will partially cancel and the extent of cancellation will increase with the ratio of the matrix particle size to the adsorbate molecular size.

ture is the presence of diagrams with shielding sets of matrix points in the latter case. Thus we might inquire under what conditions such diagrams make a small contribution to the fluid–matrix and fluid–fluid correlation functions. Examples of diagrams in $h_{ff}(r)$ which contain shielding sets are shown in Fig. 10. The two diagrams shown differ only by the presence of an $f_{mm}(r)(=\exp[-u_{mm}(r)/kT]-1)$ bond between the two matrix points. If the matrix–matrix interaction is a hard sphere potential (or any short ranged and steeply repulsive potential) we can expect a cancellation between the contributions to the sum of these two diagrams for overlapping configurations of the matrix particles where $f_{mm}(r)=-1$. (This is analogous to the approximate cancellation of the diagrams neglected in the Percus–Yevick approximation for short ranged repulsive potentials.) If the matrix particles are very much larger than the fluid particles then the contribution from overlapping configurations of the matrix particles will dominate both diagrams and in the limit of a very large size ratio the cancellation should be quite complete. For every shielding set of n matrix points there are 2^n diagrams which have the same connectivity with respect to the fluid–fluid and fluid–matrix bonds but which differ by the number of $f_{mm}(r)$ bonds. This makes it possible to effect the cancellation described above for every shielding set by taking pairs of diagrams which differ only by the absence of a single $f_{mm}(r)$ bond in one of the diagrams. Strictly speaking the cancellation depends on the range of $f_{ff}(r)$ and $f_{fm}(r)$ relative to that of $f_{mm}(r)$. If the fluid–fluid and fluid–matrix interactions are also short ranged then the cancellation will occur for smaller size ratios. Thus we should expect the cancellation to occur for quite modest size ratios for hard sphere systems and large size ratios for systems with Lennard-Jones interactions such as our M1 model.

VI. ADSORPTION ISOTHERMS FROM INTEGRAL EQUATION THEORY

In Fig. 11 we show adsorption isotherms at two temperatures as computed from Eqs. (15) and (23) and from GCMC simulations for the M1 model. At the higher temperature, $T^*=2$, both approximations give quite good results. Equation (23) seems to be the more accurate route especially at the lower temperature. We have no *a priori*

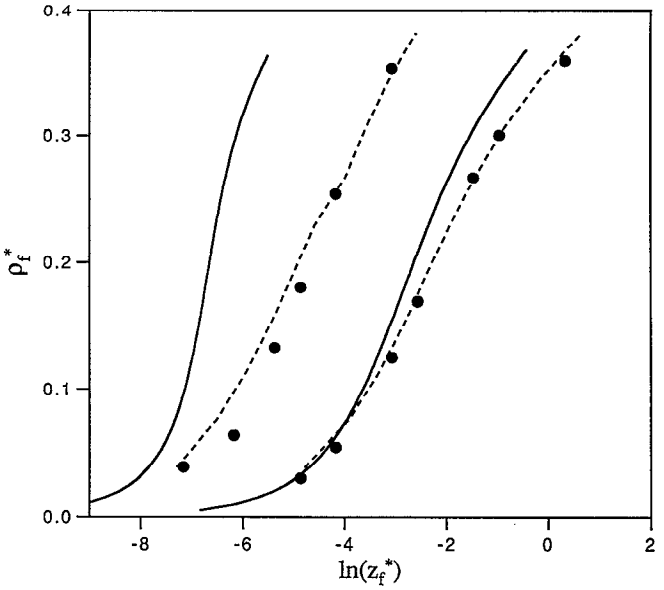

FIG. 11. Adsorption isotherms for the M1 model as obtained from the GCMC simulations (points) of Ref. 6, from Eq. (15) (solid line) and from Eq. (23) (dashed line). The data to the right of the figure are for $T^*=2$ and those to the left are for $T^*=1.2$.

reason for anticipating this result and in some respects Eq. (15) should be regarded as a more theoretically sound route in view of the somewhat *ad hoc* approximations involved in calculating μ^{ideal} via Eq. (21). Perhaps there is some cancellation of errors which accounts for the greater accuracy of Eq. (23).

Figure 12 shows the adsorption isotherm for the M2 hard sphere model. In this case we see that Eq. (23) gives

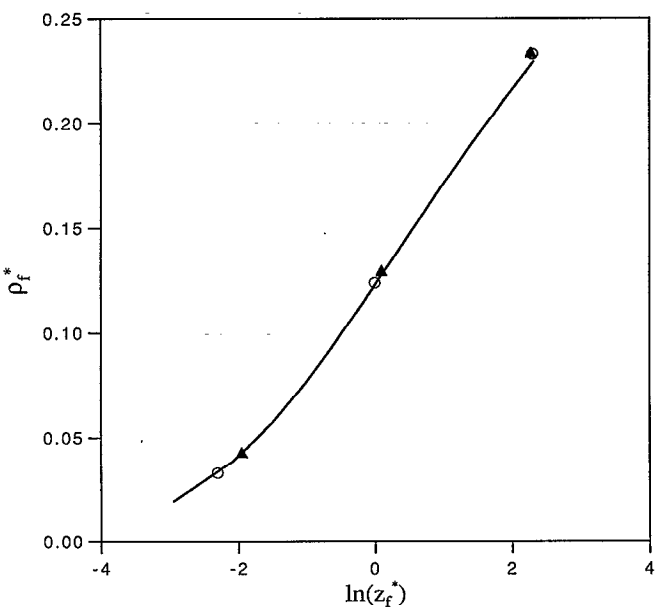

FIG. 12. Adsorption isotherm for the M2 model as obtained from GCMC (open circles) and from Eq. (23) (solid line). The filled triangles correspond to the adsorption isotherm as obtained from the equation of state for mixtures of hard spheres of Mansoori *et al.* (Ref. 25).

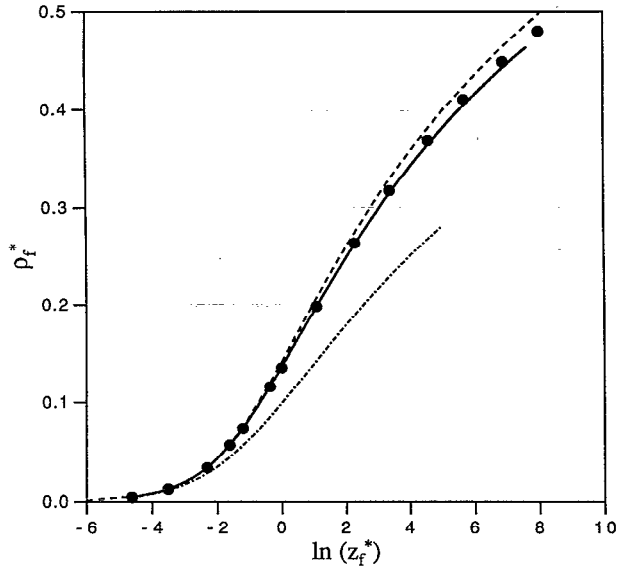

FIG. 13. Adsorption isotherm for the M3 model as obtained from GCMC (filled circles), from Eq. (15) (solid line), from the virial route of Fanti *et al.* (Ref. 3) (dot–dashed line), and from the virial route with the fluid–matrix term removed (dashed line).

very good results. In fact results of comparable accuracy are obtained from Eq. (15). In the previous section we showed that when the size ratio is large then the structure of the adsorbed fluid is very similar to that in the equilibrium binary mixture. To explore whether this similarity extends also to thermodynamic properties, we have computed the chemical potential of the fluid in the binary mixture for the M2 model by using the equation of state for mixtures of hard spheres.[25,26] The results are also shown in Fig. 12. The surprising fact is that the chemical potential of the fluid is very much the same in the porous media and in the equilibrium mixture.

Figure 13 shows the adsorption isotherm for the M3 model from simulation and various theoretical routes. The agreement with theory is again very good. We have also shown the results obtained by using the virial route to Ω_f of Fanti *et al.*[3–5] In this case we used the distribution functions from the simulation. If the virial route to Ω_f was correct then these results should be the same as those obtained directly in the simulation. No other approximations have been made. The difference between these two isotherms is clear evidence of thermodynamic inconsistency. We therefore believe that Eq. (10) is incorrect. Interestingly, if we remove the fluid–matrix term from Eq. (10) much better agreement is obtained, as is shown by the dashed line in Fig. 13. It is perhaps relevant that the fluid–matrix correlation function does not appear explicitly in Eq. (15) which in some sense is the analog of a compressibility route to Ω_f.

VII. SUMMARY AND CONCLUSIONS

The MGOZ equations along with the PY closure have been used to obtain the structure of a fluid in a random porous media. Several models have been considered. We have performed an extensive comparison of results from the MGOZ equation with computer simulation results[6] for a model in methane in silica. Moreover, some additional computer simulation results for hard sphere models have been generated. The comparison between theoretical and simulation results reveals that the MGOZ equation constitutes a reliable tool to determine the structure, internal energy and Henry's constant of the fluid in the porous medium.

In order to calculate adsorption isotherms it is necessary to establish a relationship between the chemical potential and the average density of the fluid in the porous material. One route to this is through the calculation of the grand potential, Ω_f, as a function of the fluid density, and then application of the Gibbs adsorption isotherm. We have shown that the virial route to Ω_f in the form suggested by Fanti *et al.*[3–5] does not lead to thermodynamically consistent results. However by using the density functional theory formalism for the thermodynamic properties together with the structural results from the MGOZ equation in the PY approximation and some additional approximations we have been able to obtain expressions for both the grand potential and the chemical potential. In these two ways quite good results can be obtained for the adsorption isotherms of the models considered.

When the size ratio of the matrix particles to the fluid particles is large then the structure and chemical potential of the fluid in the porous media is very similar to that of an equilibrium binary mixture. This can be partly explained through a cancellation of cluster diagrams in the density expansions of the total correlation functions of the equilibrium mixture.

ACKNOWLEDGMENTS

This work has been supported by a grant from the U.S. National Science Foundation (CTS-9115297). One of us (C.V.) would like to thank the North-American–Spanish Fulbright committee for the award of a postdoctoral grant. We are grateful to R. Pospisil, S. Labik, and A. Malijevsky for providing us with a copy of their program for solving the OZ equations of a binary mixture. We are also grateful to J. Given and G. Stell for providing a copy of Ref. 8 prior to publication.

[1] W. G. Madden and E. D. Glandt, J. Stat. Phys. **51**, 537 (1988).
[2] W. G. Madden, J. Chem. Phys. **96**, 5422 (1992).
[3] L. A. Fanti, E. D. Glandt, and W. G. Madden, J. Chem. Phys. **93**, 5945 (1990).
[4] L. A. Fanti and E. D. Glandt, J. Colloid Interface Sci. **135**, 385 (1990).
[5] L. A. Fanti and E. D. Glandt, J. Colloid Interface Sci. **135**, 396 (1990).
[6] R. D. Kaminsky and P. A. Monson, J. Chem. Phys. **95**, 2936 (1991).
[7] J. D. MacElroy and K. Raghavan, J. Chem. Phys. **93**, 2068 (1990).
[8] J. Given and G. Stell, J. Chem. Phys. **97**, 4573 (1992).
[9] J. K. Percus and G. J. Yevick, Phys. Rev. **110**, 1 (1958).
[10] J. L. Lebowitz and J. K. Percus, Phys. Rev. **144**, 251 (1966).
[11] J. G. Kirkwood, J. Chem. Phys. **3**, 300 (1935).
[12] R. J. Baxter, J. Chem. Phys. **47**, 4855 (1967); **52**, 4559 (1970).
[13] R. Evans, Course of Lectures at Les Houches School on Liquids at Interfaces, 1988.
[14] R. Evans, Adv. Phys. **28**, 143 (1979).
[15] P. Tarazona, Phys. Rev. A **31**, 2632 (1985).
[16] M. Baus, J. Phys. Condensed Matter. **2**, 2111 (1990).

[17]S. D. Lee, J. Chem. Phys. **87**, 4972 (1987).
[18]S. Labik, A. Malijevsky, and P. Vonka, Mol. Phys. **56**, 709 (1985).
[19]S. W. Rick and A. D. J. Haymet, J. Chem. Phys. **90**, 1188 (1989).
[20]C. Vega, S. Lago, R. Pospisil, S. Labik, and A. Malijevsky, J. Phys. Chem. **96**, 1895 (1992).
[21]S. Torquato, J. Chem. Phys. **85**, 4622 (1986).
[22]D. Henderson, F. F. Abraham, and J. A. Barker, Mol. Phys. **31**, 1291 (1976).
[23]J. J. Brey and A. Santos, J. Chem. Phys. **79**, 4652 (1983).
[24]J. A. Barker and D. Henderson, J. Chem. Phys. **47**, 4714 (1967).
[25]G. A. Mansoori, N. F. Carnahan, K. E. Starling, and T. W. Leland, J. Chem. Phys. **54**, 1523 (1971).
[26]T. Boublik, J. Chem. Phys. **63**, 4084 (1975).
[27]K. P. Shukla, M. Luckas, H. Marquardt, and K. Lucas, Fluid Phase Equil. **26**, 129 (1986).
[28]A. Lofti and J. Fischer, Mol. Phys. **66**, 199 (1989).
[29]J. E. Lane and T. H. Spurling, Aust. J. Chem. **33**, 231 (1980).